Supporting Information

Th@C_2(14)-C_{86} and Th@C_3(18)-C_{86}: two missing C_{86} isomers stabilized by the encapsulation of thorium

Jiawei Qiu,‡[a] Lihao Zheng,‡[a] Yannick Roselló,‡[b] Khaoula Merimi,[b] Yang-Rong Yao,[c] Zhengkai Cao,[a] Zhiwen He,[a] Josep M. Poblet,[b] Antonio Rodríguez-Fortea,[b] and Ning Chen,*[a]*

[a] College of Chemistry, Chemical Engineering and Materials Science, and State Key Laboratory of Radiation Medicine and Protection, Soochow University, Suzhou, Jiangsu 215123, P.R. China.

[b] Departament de Química Física i Inorgànica. Universitat Rovira i Virgili, Marcel·lí Domingo 1, 43007 Tarragona, Spain.

[c] Department of Chemistry and Biochemistry, University of Texas at El Paso, El Paso, Texas 79968, United States

[a] E-mail: chenning@suda.edu.cn

[b] E-mail: antonio.rodriguezf@urv.cat

‡These authors contribute equally to this work.

Table of Contents

High performance liquid chromatography (HPLC) separation process of Th@C_2(14)-C_{86} Toluene was used as mobile phase in the multiple-step HPLC procedure. The first step was performed on a Buckyprep-M column (25 mm × 250 mm, Cosmosil Nacalai Tesque) (Fig. S1 (a)). The fraction from 28.5 to 33 min (marked in blue) containing Th@C_2(14)-C_{86} was collected and then injected into the 5PYE column (10 mm × 250 mm, Cosmosil, Nacalai Tesque) for the second step. In the second step, the fraction from 27.7 to 32.8 min (marked in green) was collected for the next step of HPLC separation (Fig. S1 (b)). The third step was conducted on a 5PBB column (10 mm × 250 mm, Cosmosil, Nacalai Tesque) and the fraction from 125.3 to 145 min (marked in purple) was collected (Fig. S1 (c)). Then, this fraction was injected into a Buckyprep column (10 mm × 250 mm, Cosmosil, Nacalai Tesque) in recycle mode for the fourth step. After that, the fraction marked in green, namely pure Th@C_2(14)-C_{86}, was finally obtained (Fig. S1 (d)). Fig. S1 (e) shows the purity of the isolated Th@C_2(14)-C_{86}.

High performance liquid chromatography (HPLC) separation process of Th@C_3(18)-C_{86} Toluene was used as mobile phase in the multiple-step HPLC procedure. The first step was performed on a Buckyprep-M column (25 mm × 250 mm, Cosmosil Nacalai Tesque) (Fig. S2 (a)). The fraction from 28.5 to 33 min (marked in blue) containing Th@C_3(18)-C_{86} was collected and then injected into the 5PYE column (10 mm × 250 mm, Cosmosil, Nacalai Tesque) for the second step. In the second step, the fraction from 27.7 to 32.8 min (marked in green) was collected for the next step of HPLC separation (Fig. S2 (b)). The third step was conducted on a 5PBB column (10 mm × 250 mm, Cosmosil, Nacalai Tesque) and the fraction from 110 to 120 min (marked in deep blue) was collected (Fig. S2 (c)). Then, this fraction was injected into a Buckyprep column (10 mm × 250 mm, Cosmosil, Nacalai Tesque) for the fourth step. After that, the fractions marked in pink were collected and then injected into the Buckyprep column in recycle mode for the fifth step (Fig. S2 (d)). Finally, the fraction marked in red, namely pure Th@C_3(18)-C_{86}, was finally obtained (Fig. S2 (e)). Fig. S2 (f) shows the purity of the isolated Th@C_3(18)-C_{86}. Unfortunately, we were not able to characterize the other fraction separated in step 5, which is another isomer of Th@C_{86}.

High performance liquid chromatography (HPLC) separation process of Th@C_1(11)-C_{86}. Toluene was used as mobile phase in the multiple-step HPLC procedure. The first step was performed on a Buckyprep-M column (25 mm × 250 mm, Cosmosil Nacalai Tesque) (Fig. S3 (a)). The fraction from 28.5 to 33 min (marked in blue) containing Th@C_1(11)-C_{86} was collected and then injected into the 5PYE column (10 mm × 250 mm, Cosmosil, Nacalai Tesque) for the second step. In the second step, the fraction from 27.7 to 32.8 min (marked in green) was collected for the next step of HPLC separation (Fig. S3 (b)). Then, this fraction was injected into the 5PBB column (10 mm × 250 mm, Cosmosil, Nacalai Tesque) for the third step (Fig. S3 (c)). We collected the fraction from 125.3 to 145 min (marked in purple). In the fourth step, this fraction was injected into Buckyprep column (10 mm × 250 mm, Cosmosil, Nacalai Tesque) in recycle mode. After that, the fraction marked in deep blue, namely pure Th@C_1(11)-C_{86}, was finally obtained (Fig. S3 (d). Fig. S3 (e) shows the purity of the isolated Th@C_1(11)-C_{86}.

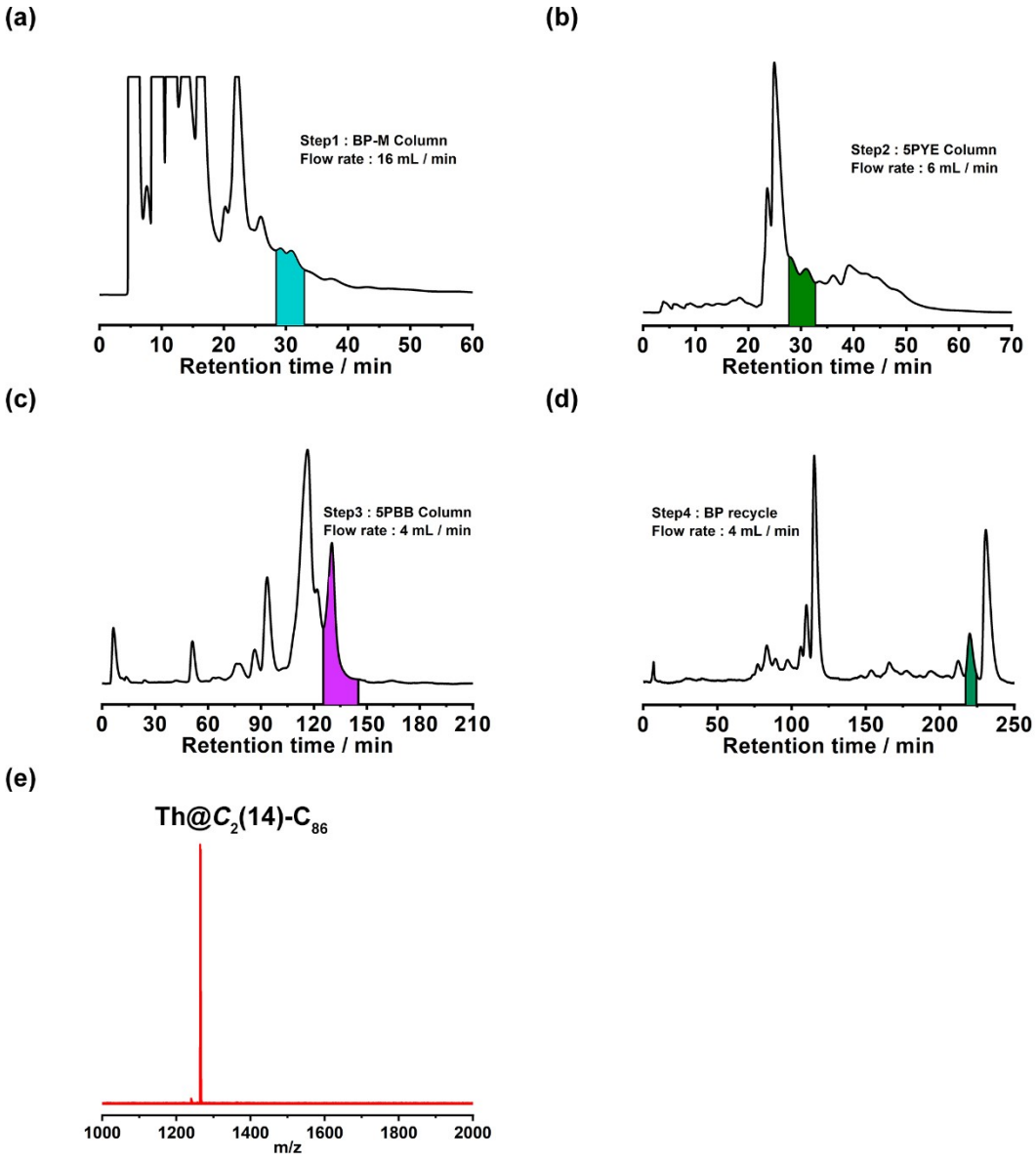

Fig. S1. (a-d) HPLC profiles showing the isolation procedures of Th@C_2(14)-C_{86}. (e) The MALDI-TOF mass spectrum of the purified Th@C_2(14)-C_{86}.

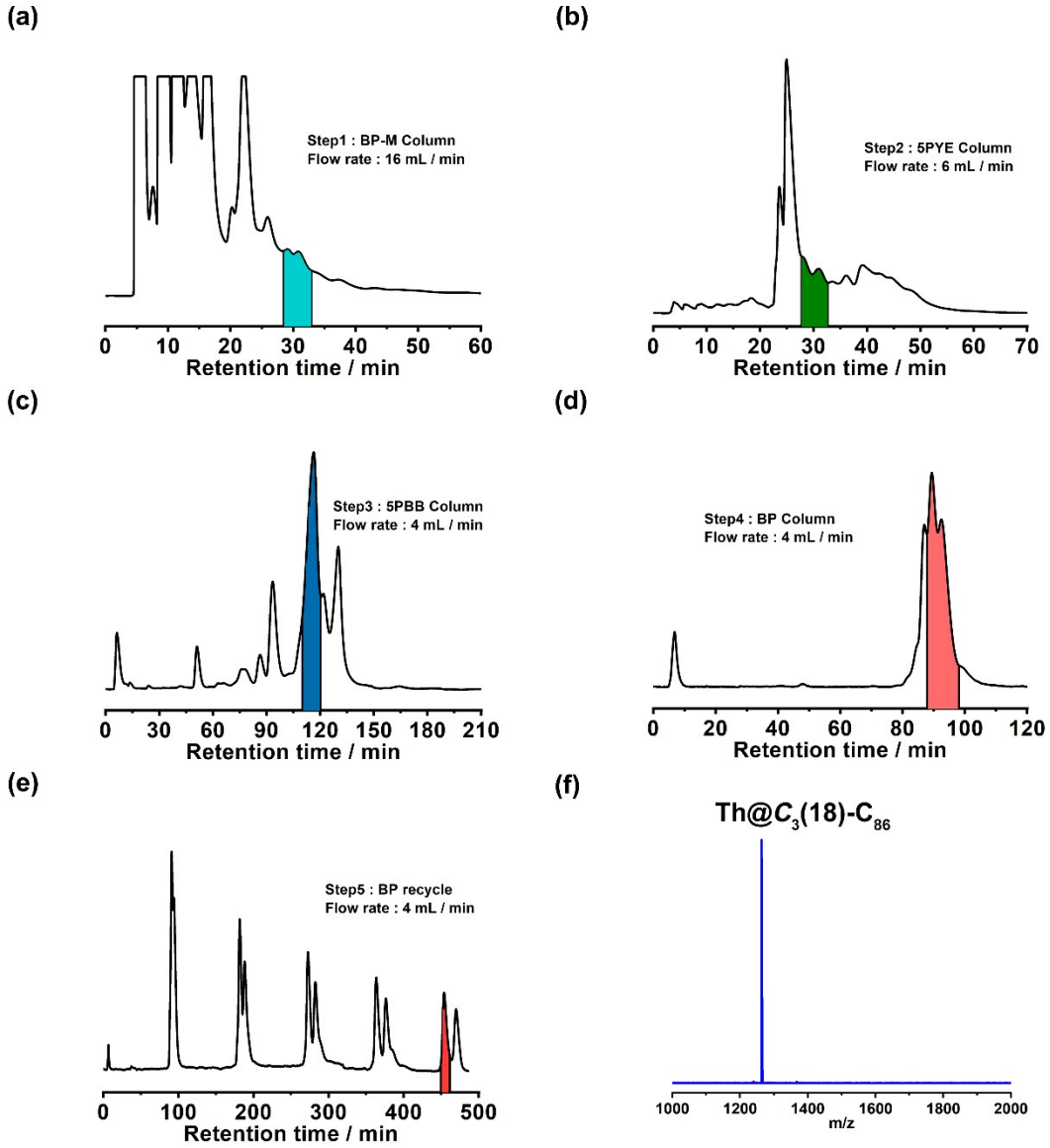

Fig. S2. (a-e) HPLC profiles showing the isolation procedures of Th@C_3(18)-C_{86}. (f) The MALDI-TOF mass spectrum of the purified Th@C_3(18)-C_{86}.

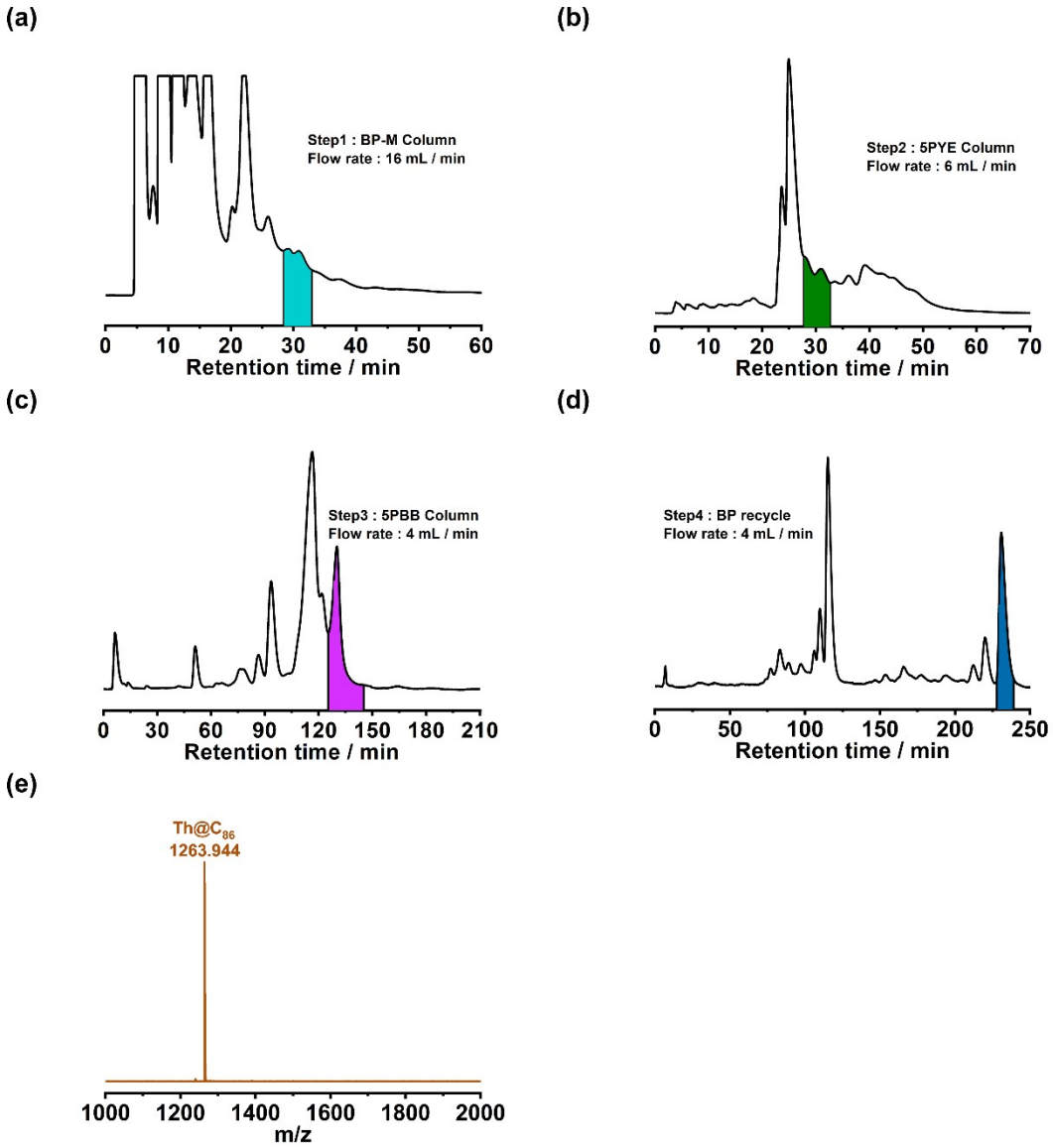

Fig. S3. (a-e) HPLC profiles showing the isolation procedures of Th@C_1(11)-C_{86}. (f) The MALDI-TOF mass spectrum of the purified Th@C_1(11)-C_{86}.

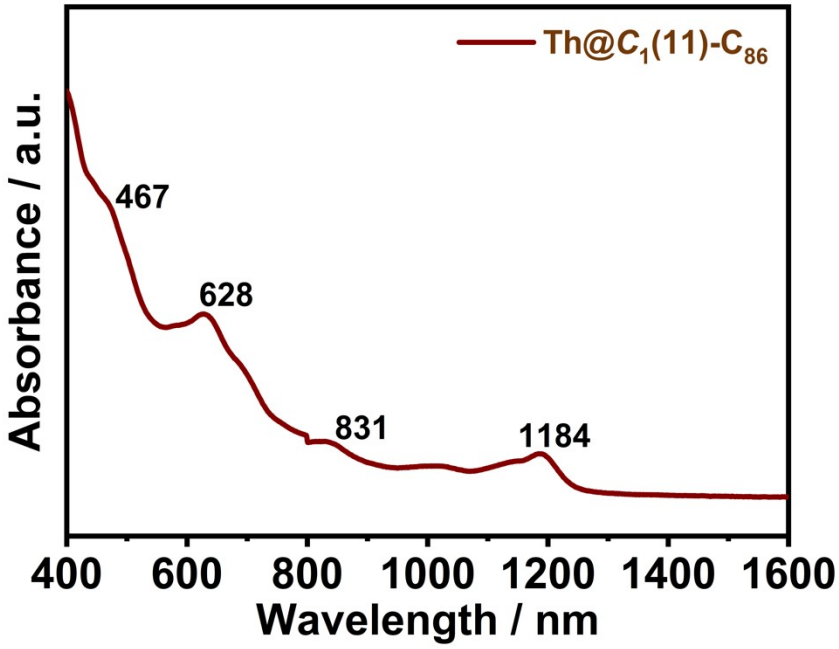

Fig. S4. UV-vis-NIR absorption spectrum of Th@C_1(11)-C_{86} corresponding to Fig. S3

As shown in Fig. S4, the UV-vis-NIR spectrum of the purified Th@C_{86} isomer (see Fig. S3) shows absorptions at 467, 628, 831 and 1184 nm, respectively, which is very similar to that of previously reported Th@C_1(11)-C_{86}.[1] Thus, this Th@C_{86} isomer should be Th@C_1(11)-C_{86} as well.

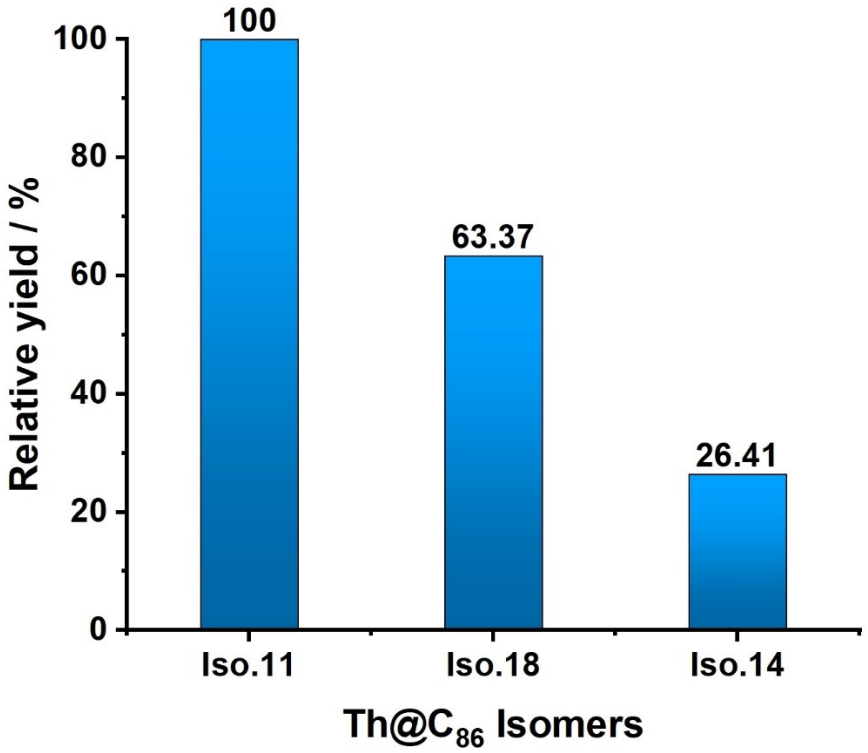

Fig. S5. The bar chart of the relative yield (in %) of Th@C_1(11)-C_{86} (Iso. 11), Th@C_3(18)-C_{86} (Iso. 18) and Th@C_2(14)-C_{86} (Iso. 14). The number in the top of each bar is the relative yield (in %) of corresponding Th@C_{86} isomers.

According to the experimental results of HPLC separation, the estimated yield of these two new isomers, Th@C_2(14)-C_{86} and Th@C_3(18)-C_{86}, is ca. 0.03 mg and 0.07 mg, respectively. Compared with Iso.14 and Iso. 18, the yield of Iso.11 is the highest, which is ca. 0.11 mg. For clarity, we present their relative yield in the term of bar chart.

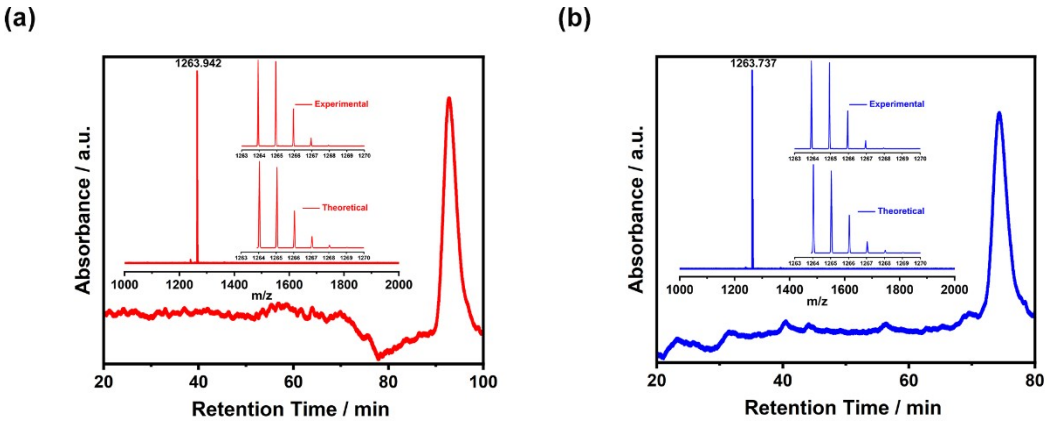

Fig. S6. HPLC chromatogram of purified Th@C_2(14)-C_{86} (a) and Th@C_3(18)-C_{86} (b) on a Buckyprep column with toluene as the eluent (HPLC conditions: λ = 310 nm; flow rate = 4 mL/min). The insets show the positive-ion mode MALDI-TOF mass spectra and expansions of the corresponding experimental isotopic distribution of Th@C_2(14)-C_{86} (a) and Th@C_3(18)-C_{86} (b) in comparison with the theoretical one.

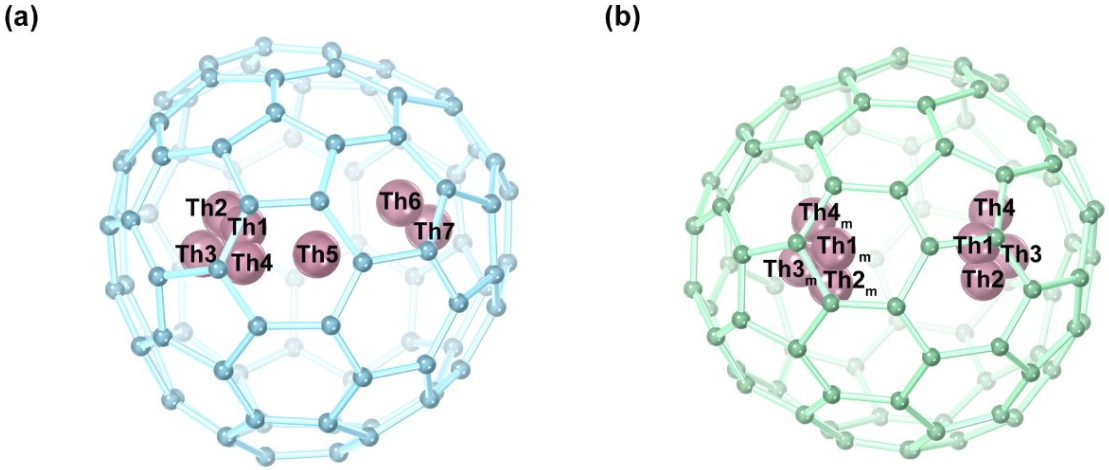

Fig. S7. Drawing of all the Th disordered sites and their mirror-related counter-parts (Th_m) in Th@C_2(14)-C_{86} (a) and Th@C_3(18)-C_{86} (b).

Table S1. Atom occupancy of metal sites in Th@C_2(14)-C_{86}.

Metal site	Th1	Th2	Th3	Th4	Th5	Th6	Th7
Occupancy	0.571(2)	0.154(2)	0.0779(11)	0.146(2)	0.0128(7)	0.0253(8)	0.0121(7)

Table S2. Atom occupancy of metal sites in Th@C_3(18)-C_{86}.

Metal site	Th1/$Th1_m$	Th2/$Th2_m$	Th3/$Th3_m$	Th4/$Th4_m$
Occupancy	0.3611(16)	0.0524(14)	0.0197(7)	0.0667(9)

Table S3. Crystallographic information of Th@C_2(14)-C_{86}·[Ni^{II}(OEP)]

	Th@C_2(14)-C_{86}·[Ni^{II}(OEP)]
Empirical formula	$C_{132.27}H_{53.92}N_4NiS_{0.69}Th$
Formula weight	2011.87
Crystal system	monoclinic
Space group	$P2_1/c$
a, Å	19.9526(11)
b, Å	15.0974(7)
c, Å	25.5792(12)
α, deg	90
β, deg	93.998(3)
γ, deg	90
Volume, Å^3	7686.5(7)
Z	4
T, K	100(2)
F(000)	4018
ρ, g·cm^{-3}	1.739
θ, deg	3.401- 72.119
R_1(all data)	0.0787
wR_2(all data)	0.1703
$R_1(I > 2.0\sigma(I))$	0.0625
$wR_2(I > 2.0\sigma(I))$	0.1585
parameters	2134
Goodness-of-fit indicator	1.083
R_{int}	0.0625

Table S4. Crystallographic information of Th@C_3(18)-C_{86}·[Ni^{II}(OEP)]

	Th@C_3(18)-C_{86}·[Ni^{II}(OEP)]
Empirical formula	$C_{122}H_{44}N_4NiTh$
Formula weight	1856.36
Crystal system	monoclinic
Space group	*C*2/*m*
a, Å	25.3709(13)
b, Å	15.2000(8)
c, Å	19.9741(10)
α, deg	90
β, deg	96.512(2)
γ, deg	90
Volume, Å^3	7653.1(7)
Z	4
T, K	100(2)
F(000)	3688
ρ, g·cm^{-3}	1.611
θ, deg	2.226-77.468
R_1(all data)	0.0797
wR_2(all data)	0.1437
$R_1(I > 2.0\sigma(I))$	0.0563
$wR_2(I > 2.0\sigma(I))$	0.1314
parameters	1008
Goodness-of-fit indicator	1.035
R_{int}	0.0730

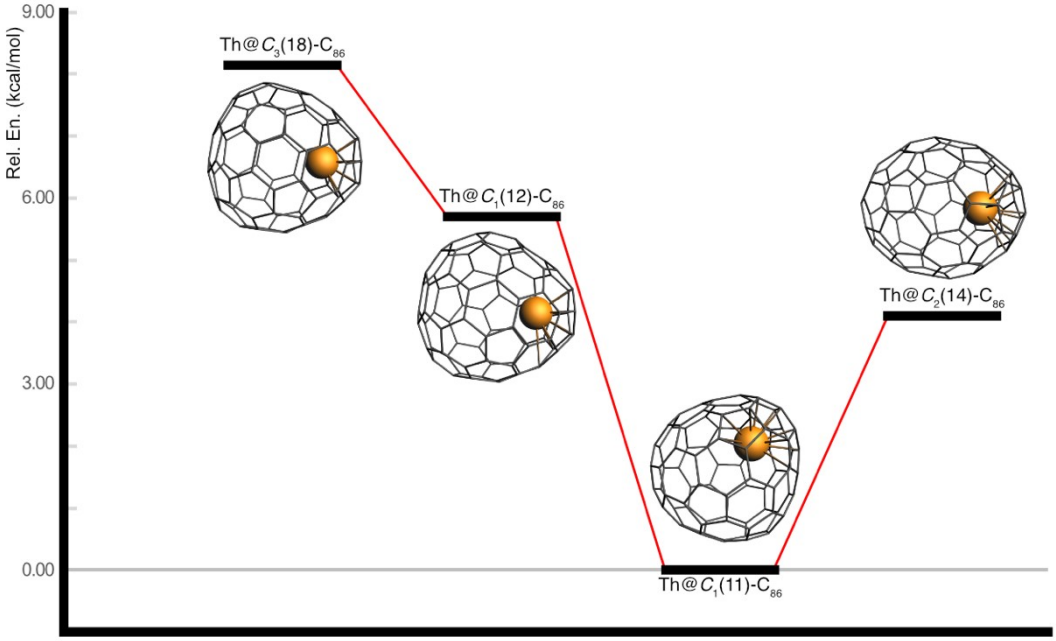

Fig. S8. Relative energy for isomers Th@C_3(18)-C_{86}, Th@C_1(12)-C_{86}, Th@C_1(11)-C_{86} and Th@C_2(14)-C_{86}. All structures are interconnected by SW transformations as depicted in Fig. S9.

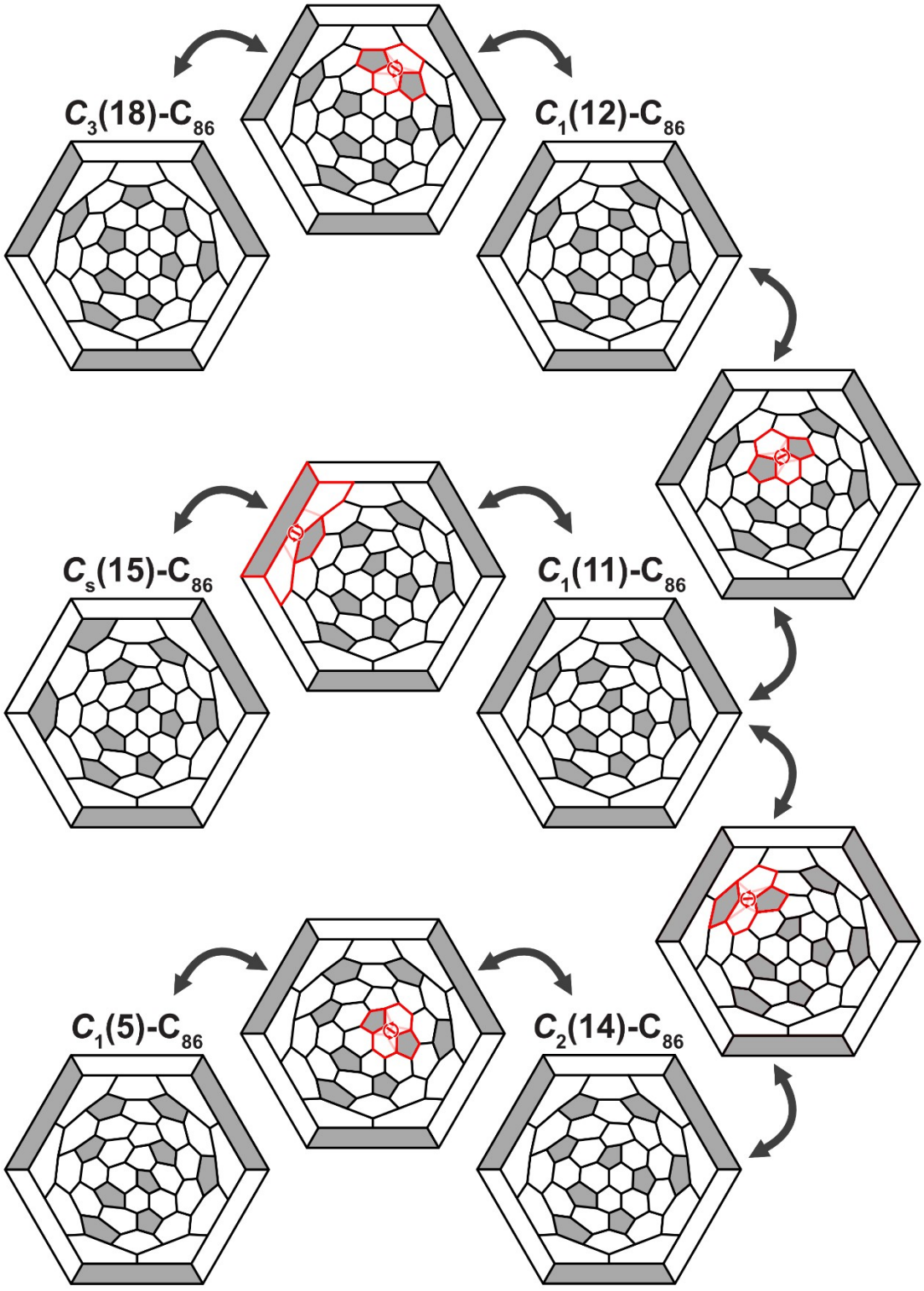

Fig. S9. Stone-Wales transformations between different isomers of Th@C_{86}.

Table S5. Relative energies (kcal mol^{-1}) of the 19 IPR Th@C_{86} isomers computed with different density functionals (hybrid PBE0 and GGA PBE and GGA BP86). BP86 results are from our previous work.[1]

Isomer	PBE0	PBE	BP86[1]
Th@C_1(11)-C_{86}	0.0	0.0	0.0
Th@C_s(15)-C_{86}	2.6	1.8	1.9
Th@C_2(14)-C_{86}	4.1	3.7	3.3
Th@C_1(5)-C_{86}	4.4	4.5	
Th@C_1(12)-C_{86}	5.7	9.2	
Th@C_2(17)-C_{86}	6.4	4.8	4.7
Th@C_{2v}(9)-C_{86}	7.4	9.4	7.3
Th@C_3(18)-C_{86}	8.1	7.1	
Th@C_2(6)-C_{86}	10.7	9.7	
Th@C_s(16)-C_{86}	11.1	10.7	
Th@C_1(13)-C_{86}	13.3	10.5	10.6
Th@C_1(7)-C_{86}	13.9	11.8	
Th@C_s(4)-C_{86}	16.5	15.4	
Th@C_s(8)-C_{86}	19.2	16.3	13.8
Th@D_3(19)-C_{86}	21.6	19.9	20.1
Th@C_{2v}(10)-C_{86}	23.3	20.3	
Th@C_2(3)-C_{86}	23.4	20.0	
Th@C_1(1)-C_{86}	23.5	22.7	
Th@C_2(2)-C_{86}	51.3	46.2	

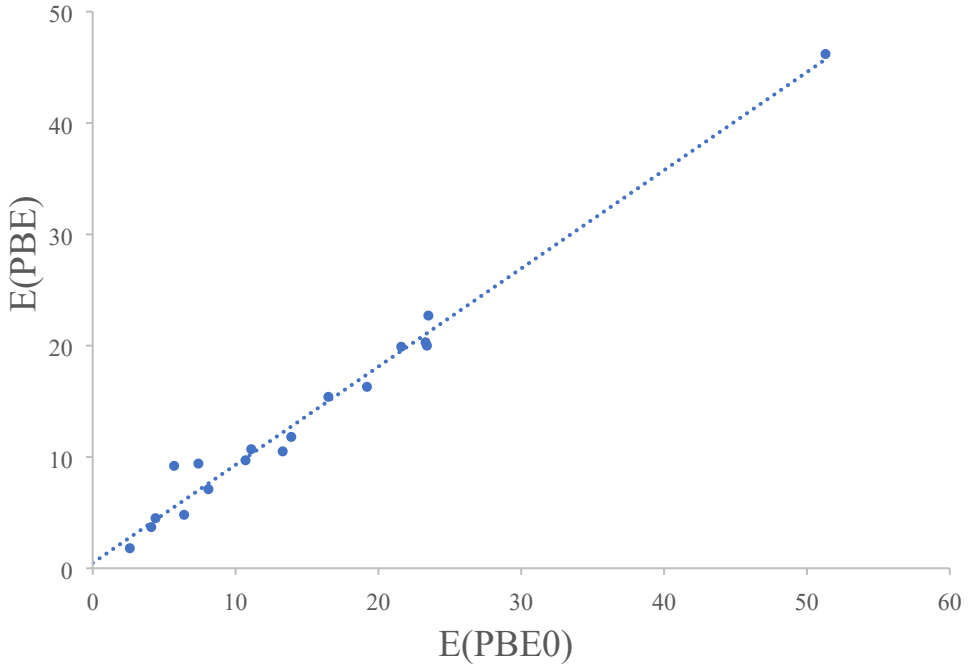

Fig. S10. Plot of the PBE relative energies (in kcal mol^{-1}) with respect to the PBE0 energies of the 19 IPR Th@C_{86} isomers.

Small changes in relative energies due to for example using different density functionals might have consequences in the predicted molar fractions. This is why we have compared the results of hybrid PBE0 functional (the one used in Fig. 3) with PBE and BP86 (from our previous work[1]). Even though small changes in the relative energies led to changes in the relative stability order of some isomers (see Table S5), the "main" order is kept, especially for the lowest-energy isomers. When plotting the PBE vs PBE0 energies (Fig. S10), the point that deviates the most from the fitted straight line is isomer 12, which shows the fifth lowest energy in PBE0 and the seventh in PBE. Relative BP86 energies are in general very similar to PBE energies (Table S5).

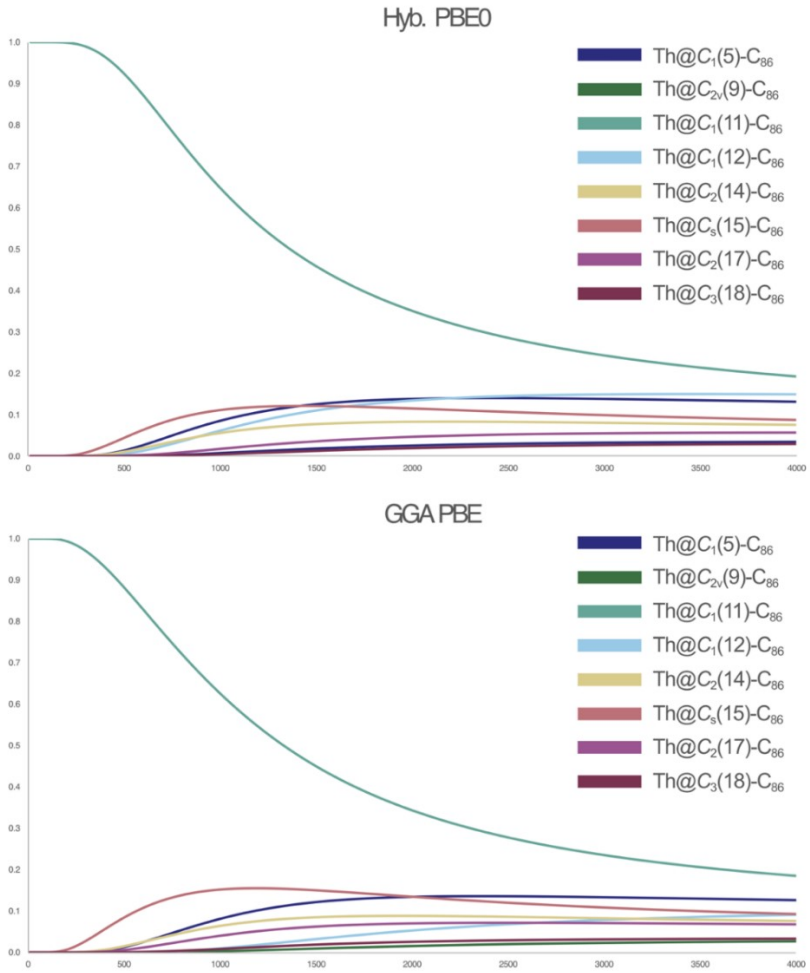

Fig. S11 Computed molar fraction as a function of the temperature (K) using the free encapsulating model (FEM)[2-4] for the optimized isomers of Th@C_{86} using PBE0 and PBE energies.

Even though this unavoidable differences in the relative energies when changing the density functional, we have seen that the predicted molar fractions keep their main shapes. Regardless the functional, (i) the most abundant isomer is Th@C_1(11)-C_{86}; (ii) isomers Th@C_s(15)-C_{86}, Th@C_1(5)-C_{86} and Th@C_2(14)-C_{86} are rather abundant in the range 1500-2000 K; and (iii) isomer Th@C_3(18)-C_{86} is predicted to have low abundance. The main difference comes from isomer Th@C_1(12)-C_{86}, which is predicted to be rather abundant at PBE0 level and much less abundant at PBE level. Therefore, we can state that the main conclusions of the work do not change when considering these different functionals.

Reference:

1. Y. Wang, R. Morales-Martínez, W. Cai, J. Zhuang, W. Yang, L. Echegoyen, J. M. Poblet, A. Rodríguez-Fortea and N. Chen, Th@C_1(11)-C_{86}: an actinide encapsulated in an unexpected C_{86} fullerene cage, Chem. Commun., 2019, **55**, 9271-9274.
2. Z. Slanina and L. Adamowicz, On the relative stabilities of dodecahedron-shaped and bowl-shaped structures of C_{20}, Thermochim. Acta, 1992, **205**, 299-306.
3. Z. Slanina and S. Nagase, $Sc_3N@C_{80}$: Computations on the Two-Isomer Equilibrium at High Temperatures, ChemPhysChem, 2005, **6**, 2060-2063.
4. Z. Slanina, S.-L. Lee, F. Uhlík, L. Adamowicz and S. Nagase, Computing relative stabilities of metallofullerenes by Gibbs energy treatments, Theor. Chem. Acc., 2007, **117**, 315-322.